Modeling the propagation of optical beams in three-dimensional photonic crystals

Babak Momeni,* Majid Badieirostami, and Ali Adibi

School of Electrical and Computer Engineering, Georgia Institute of Technology, Atlanta, Georgia 30332, USA
**Corresponding author: babak.momeni@osa.org*

Received December 11, 2007; accepted February 6, 2008;
posted March 18, 2008 (Doc. ID 90700); published April 28, 2008

We show that the propagation effects of optical beams in three-dimensional photonic crystal structures can be modeled using a direction-dependent effective diffractive index model. The parameters of the model (i.e., the effective diffractive indices) can be calculated using the curvatures of the band structure of the photonic crystal at the operation point. After finding these indices, the wave propagation inside the photonic crystal can be analyzed using simple geometrical optics formulas. We show that the model has good accuracy for most practical applications of photonic crystals. As an example, the application of the model for diffraction compensation in a tetragonal woodpile photonic crystal is demonstrated. © 2008 Optical Society of America

OCIS codes: 050.1940, 160.5298, 070.7345.

1. INTRODUCTION

The idea of periodic dielectric structures, known as photonic crystals (PCs), for engineering the photonic density of states [1,2] and realizing synthetic optical materials [3] has stimulated considerable research activity lately. Dispersive properties of two-dimensional (2D) PCs in planar structures have shown attractive potential [4–6]. On the other hand, recent advances in the fabrication of three-dimensional (3D) PC structures, including layer-by-layer processing [7], direct laser writing by multiphoton lithography [8–10], and multibeam interference lithography [11–13] have made possible the realization of such structures for practical applications. Applications including beam shaping, dispersion control, and spectroscopy are among a variety of possibilities in which unique dispersive properties of 3D PCs can be used [14,15]. However, to design and implement these structures efficiently and systematically, it is essential to have a basic understanding of the propagation effects in 3D PCs.

The amount of memory and computation cost required in direct space-domain simulation of 3D PC structures for dispersion-based applications makes direct techniques such as the finite-difference time-domain (FDTD) method highly inefficient. A modal approach is more efficient in this case because it reduces both the required memory and the computation cost for large structures. The model can be, under certain conditions, simplified to make a direct intuitive connection between propagation effects inside PCs and those of ordinary bulk media. In particular, it has been shown recently that the propagation of light in 2D PCs can be accurately and efficiently analyzed using an effective diffractive index model [16]. The 2D diffractive index model has been successfully used to design and optimize 2D PC structures for applications such as wavelength demultiplexing [17] and diffraction compensation [18]. Here, we report the development of a 3D diffractive index model for efficient analysis of wave propagation in 3D PC structures. We show that the propagation of the electromagnetic waves (at a certain frequency, direction, and polarization) inside such structures can be modeled by two principal diffractive indices that describe the beam behavior in two directions perpendicular to the direction of propagation. We will investigate the accuracy of the model by comparing its results for different 3D PC structures with those of direct numerical simulations.

In what follows, we will develop the diffractive index model for 3D PC structures in Section 2. The model will be verified and the extent of its applicability to practical problems will be discussed in Section 3. In Section 4, the model will be used to analyze the negative diffraction effect in 3D PC structures as an example of practical dispersive applications. Concluding remarks will be given in Section 5.

2. DIFFRACTIVE INDEX MODEL FOR THREE-DIMENSIONAL PHOTONIC CRYSTALS

The problem of interest in most dispersive applications of PCs is the modeling of the evolution of optical beams propagating through the periodic structure. Recently, some models have been suggested to describe these effects for special cases [19,20], but a general model for 3D PCs is still missing. To analyze these structures, modal approaches can be directly used by expanding the beam over the modes of the PC structure. This, however, requires a detailed mode matching process, which is a tedious task. At the same time, in most dispersion-based applications of PCs we are not interested in the details of the beam profile inside the periodic structure. In most practical cases, an accurate description of the behavior of the envelope of the optical beam is the main interest. In this section, we develop an easy to use model for the analysis of the envelope of an optical beam as it propagates through a 3D PC structure. This model can also provide useful insight into the process of beam propagation through 3D PC

structures. It has been shown [14] that in 2D PCs an envelope transfer function (ETF) (using the band structure) can be defined to model the evolution of the special envelope of the beam inside the PC structure. Here, we extend this idea to define the amplitude transfer function for 3D PCs. Local quadratic approximation of the band structure at the operation point is then used to define diffractive indices that describe the diffraction of optical beams inside the PC structure at different wavelengths.

One main concept that differentiates between the 3D and the 2D PCs is the vectorial nature of the electromagnetic fields in the 3D case, which cannot be modeled using scalar quantities as in the 2D case. Nevertheless, it can be shown [21] that the polarization of the modes of 3D PC structures in most practical cases have Bloch components with well-defined transverse eigenstates. In addition, these polarization states have smooth variations over the band structure. As a result, an optical beam with limited spatial–spectral content in a 3D PC can be locally modeled using a scalar field by projecting its actual vector field over the dominant polarization state. In what follows, such a scalar model is used to develop approximate solutions; the validity of this assumption will be discussed in more detail in Sections 3 and 4.

For simplicity, we consider a tetragonal woodpile 3D PC in our derivations. The formulation can be extended readily to other lattices, and the results are not limited to the choice of lattice. Assume we have an optical beam with an initial scalar (electric or magnetic) field distribution $p_1(x,y)$ along $z=z_1$ (i.e., a plane normal to the z axis) inside the PC. We can expand this distribution over the PC modes as

$$p_1(x,y)=\frac{1}{4\pi^2}\int\int A(k_x,k_y)U_{\bar{k}}(x,y,z_1)\exp(-jk_xx-jk_yy)\times\exp(-jk_zz_1)\mathrm{d}k_x\mathrm{d}k_y, \quad (1)$$

where each PC mode is represented by an excitation amplitude [i.e., $A(k_x,k_y)$], a periodic Bloch function [i.e., $U_{\bar{k}}(x,y,z)$], and a propagation term [i.e., $\exp(-jk_xx-jk_yy-jk_zz)$], and the integration is performed over the entire 2D k_x-k_y plane. The periodic Bloch function can be expanded as a Fourier series

$$U_{\bar{k}}(x,y,z)=\sum_m\sum_n\sum_l \tilde{U}_{mnl}(k_x,k_y,k_z)\times\exp[-j(mK_xx+nK_yy+lK_zz)], \quad (2)$$

in which, $K_x=2\pi/a_x$, $K_y=2\pi/a_y$, and $K_z=2\pi/a_z$ are the reciprocal lattice vectors of the PC in the k domain (a_x, a_y, and a_z are the corresponding lattice constants in the x, y, and z directions, respectively). The initial scalar field expansion, thus, can be written as

$$p_1(x,y)=\frac{1}{4\pi^2}\int\int A(k_x,k_y)\left(\sum_m\sum_n\sum_l \tilde{U}_{mnl}(k_x,k_y)\times\exp[-j(k_x+mK_x)x]\exp[-j(k_y+nK_y)y]\times\exp[-j(k_z+lK_z)z_1]\right)\mathrm{d}k_x\mathrm{d}k_y, \quad (3)$$

where $\tilde{U}_{mnl}(k_x,k_y)$ represents the Fourier expansion coefficient of the periodic Bloch function. Note that since this expansion corresponds to a specific operation frequency, by fixing k_x and k_y, the third component of the wave vector of the PC mode, k_z, will be known [i.e., k_z is a function of k_x and k_y, or $k_z=k_z(k_x,k_y)$], and this fact has been used in Eq. (3)].

The 2D spatial Fourier transform of the field distribution, $p_1(x,y)$ can be calculated as

$$P_1(k_x,k_y)=\int\int p_1(x,y)\exp(jk_xx)\exp(jk_yy)\mathrm{d}x\mathrm{d}y=\sum_m\sum_n\sum_l A(k_x',k_y')\tilde{E}_{mnl}(k_x',k_y')\times\exp\{j[k_z(k_x',k_y')+lK_z]z_1\}\Big|_{\substack{k_x'=k_x-mK_x\\k_y'=k_y-nK_y}}, \quad (4)$$

$$P_1(k_x,k_y)=\sum_m\sum_n\sum_l A(k_x-mK_x,k_y-nK_y)\times\tilde{E}_{mnl}(k_x-mK_x,k_y-nK_y)\times\exp\{j[k_z(k_x-mK_x,k_y-nK_y)+lK_z]z_1\}. \quad (5)$$

Assuming that the beam profile covers a limited spectrum around $(k_x,k_y)=(k_{x0},k_{y0})$, we can extract the envelope of the beam by filtering out the high-frequency portion of the spectrum around (k_{x0},k_{y0}) and moving it to the baseband by shifting the spectrum by $-k_{x0}$ and $-k_{y0}$ in the k_x and k_y directions, respectively [14]. The resulting spectrum of the envelope, represented by $\bar{P}_1(k_x,k_y)$, is

$$\bar{P}_1(k_x,k_y)=A(k_x+k_{x0},k_y+k_{y0})\exp[jk_z(k_x+k_{x0},k_y+k_{y0})z_1]\times\left(\sum_l \tilde{E}_{00l}(k_x+k_{x0},k_y+k_{y0})\exp(jlK_zz_1)\right). \quad (6)$$

Note that all m and $n\neq 0$ in Eq. (5) correspond to the higher spatial frequency terms corresponding to rapid spatial variations in the length scales smaller than a PC unit cell. For the analysis of propagation of optical beams in a dispersive PC structure, the optical beam usually covers multiple unit cells, and such rapid variations will not be of interest in designing PC structures for practical applications.

At the monitoring output plane, $z=z_2$, the spectrum of the envelope of the beam can be calculated as

$$\bar{P}_2(k_x,k_y)=A(k_x+k_{x0},k_y+k_{y0})\exp[jk_z(k_x+k_{x0},k_y+k_{y0})z_2]\times\left(\sum_l \tilde{E}_{00l}(k_x+k_{x0},k_y+k_{y0})\exp(jlK_zz_2)\right). \quad (7)$$

If $z_2-z_1=2\pi q/K_z$ (with q being an integer), the summation term in Eqs. (6) and (7) will be exactly the same, resulting in

$$\bar{P}_2(k_x,k_y)=\bar{P}_1(k_x,k_y)\exp[jk_z(k_x+k_{x0},k_y+k_{y0})(z_2-z_1)], \quad (8)$$

which means that the effect of propagation from $z=z_1$ to $z=z_2$ on the envelope of the beam is only a phase change in the spectral domain similar to a plane-wave-type propagation with propagation constant k_z. Thus, the main effect of propagation in 3D PCs on the beam envelope is

the phase variations of the modes from the initial plane to the observation plane.

Based on Eq. (8), we can define an ETF for the structure to describe the propagation from the $z=z_1$ plane to the $z=z_2$ plane as

$$H(k_x,k_y)=\frac{\bar{P}_2(k_x,k_y)}{\bar{P}_1(k_x,k_y)}=\exp[j(z_2-z_1)k_z], \tag{9}$$

where $k_z=k_z(k_x+k_{x0},k_y+k_{y0})$ is related to k_x and k_y through the dispersion relation of the structure at the constant temporal frequency (ω) of the beam. The ETF for 3D PCs [given by Eq. (9)] is similar to what was obtained for 2D PC structures [14], with the main difference being the extension of the ETF from a single-variable function to a two-variable one. Using the analogy with propagation in bulk media, we can extend Eq. (9) to the case of beam propagation along the ζ direction (normal to the constant frequency surface at the point of operation, i.e., parallel to $\mathbf{v}_g=\nabla_{\mathbf{k}}\omega$) as

$$H(k_\xi,k_\eta)=\frac{\bar{P}_2(k_\xi,k_\eta)}{\bar{P}_1(k_\xi,k_\eta)}=\exp[-j(\zeta_2-\zeta_1)k_\zeta(k_\xi,k_\eta)], \tag{10}$$

where the coordinates ξ, η, and ζ are defined in Fig. 1.

Equation (10) can be used readily to investigate beam propagation effects for the most general case inside a 3D PC. The analogy with propagation in normal bulk media can be further utilized if we express the exponential term of the spectral response in Eq. (9) in terms of its Taylor expansion. Knowing that the diffraction of an optical beam (defined by ω and $\mathbf{k}$) inside a PC is governed by the curvatures of the constant frequency surface at the operation point, we need to first calculate the PC band curvatures at the operation point. Using the second-order approximation,

$$\begin{aligned}k_z=k_{z0}+a_2(k_x-k_{x0})+a_3(k_y-k_{y0})+a_4(k_x-k_{x0})^2\\+a_5(k_x-k_{x0})(k_y-k_{y0})+a_6(k_y-k_{y0})^2,\end{aligned} \tag{11}$$

a standard method can be adopted to find these curvatures [22]. First, we define W as the magnitude of the gradient at the operation point, given by

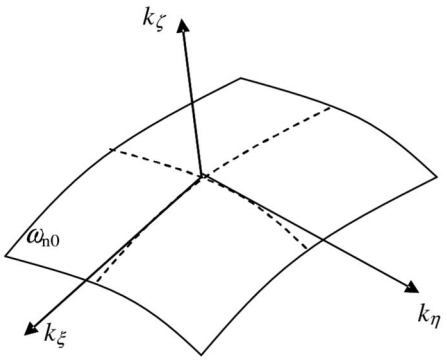

Fig. 1. Portion of an isofrequency surface (at normalized frequency ω_{n0}) of a general 3D PC in the k space is shown. The directions tangent to the surface (i.e., ξ and η) and the direction normal to the surface (ζ) are defined in the figure.

$$W=\sqrt{1+a_2^2+a_3^2}. \tag{12}$$

Then, the parameters for the first fundamental form of the surface (associated with the tangent plane) can be found as [22]

$$\begin{aligned}E&=(1+a_2^2)W,\\F&=a_2a_3W,\\G&=(1+a_3^2)W,\end{aligned} \tag{13}$$

and those of the second fundamental form (associated with the second-order curvatures) can be calculated as

$$\begin{aligned}L&=2a_4,\\M&=a_5,\\N&=2a_6.\end{aligned} \tag{14}$$

Using these relations, which are coefficients of the fundamental forms of a quadratic surface, we can calculate the Gaussian curvature as

$$K=\frac{LN-M^2}{EG-F^2}, \tag{15}$$

and the mean curvature as

$$H=\frac{1}{2}\frac{EN-2FM+GL}{EG-F^2}. \tag{16}$$

Finally, the two principal curvatures can be calculated as

$$\kappa_1=H+\sqrt{H^2-K}, \tag{17}$$

$$\kappa_2=H-\sqrt{H^2-K}. \tag{18}$$

The principal directions, $\mathbf{v}_i$, can be calculated by inserting these principal curvatures in the characteristic equation,

$$\begin{pmatrix}L-\kappa_iE & M-\kappa_iF\\ M-\kappa_iF & N-\kappa_iG\end{pmatrix}\mathbf{v}_i=0 \quad i=1,2, \tag{19}$$

which determines the principal directions projected on the xy plane. From these directions, we can find the two directions at the operation point on the band structure, which are normal to the gradient direction,

$$\mathbf{n}=(-a_2,-a_3,1). \tag{20}$$

The two directions obtained from this process determine the principal directions corresponding to the principal curvatures at the operation point on the band structure. Since these curvatures describe the diffraction of the optical beam inside the structure, we will refer to these two principal directions as the principal diffraction directions. Without loss of generality we assume the directions of ξ and η in Fig. 1 to be along the principal diffraction directions at the operation point. Note that in the special case that the two curvatures are equal (i.e., the degenerate case), the choice of the principal diffraction directions is arbitrary.

To summarize, for each mode of the 3D PC structure (at a given ω and $\mathbf{k}$), there are two principal diffraction directions in the plane perpendicular to the direction of group velocity for that mode. A principal diffractive index can be defined for each of these directions to describe the diffraction of an optical beam along that specific direction. Based on the analogy with bulk media, we can find the principal diffractive indices $(n_{d\xi}, n_{d\eta})$ at the operation point as

$$n_{d\xi} = \frac{1}{k_0 \kappa_1},$$

$$n_{d\eta} = \frac{1}{k_0 \kappa_2}. \tag{21}$$

The same phenomenon of anisotropic diffraction, in principle, occurs in ordinary anisotropic media as well, but the extent of the contrast between the two principal diffractive indices can be much larger in 3D PCs (for instance they can have opposite signs), and the beam propagation effects in 3D PCs can show practically significant effects from a device point of view. Equation (21) is the final result of our model. To implement this model for an arbitrary 3D PC, we need to first calculate the 3D band structure, which can be efficiently done by analyzing one unit cell of the PC structure using a standard technique such as plane wave expansion or FDTD. Then, we can calculate the curvatures of the isofrequency surface of the band structure at the operation point of interest. The advantage of this model is that the calculation of curvatures is fast (much faster than the analysis of wave propagation in even a small 3D PC). Furthermore, once the diffractive indices are calculated, they can be readily used to study propagation effects of optical beams for different propagation lengths and in a variety of applications of that PC structure.

3. RESULTS

To verify the applicability of our approximate diffractive index model, we investigate the propagation of a Gaussian beam inside a woodpile PC structure with a tetragonal unit cell [as shown in Fig. 2(a)] with $f_x = f_y = 0.3$, $f_z = 0.5$, and $a_z = 2.4a_x = 2.4a_y = 2.4a$. The relative permittivity of the material used for fabricating the 3D PC is assumed to be $\varepsilon_r = 2.5$ throughout this paper, which is the typical value in structures realized in polymer-based PCs. We assume the incident wave to be a Gaussian beam coming from a homogeneous bulk material (with $\varepsilon_r = 2.5$) at $\alpha = 38°$ and $\phi = 0°$ [i.e., propagation in the xz plane in Fig. 2(b)], where α is the angle between the incident wave vector and the z axis, and ϕ is the angle between the plane of incidence and the x axis as shown in Fig. 2(b). For this lattice, the dominant polarizations of the PC modes are very close to the conventional transverse electric (TE) and transverse magnetic (TM) polarizations [21]. By direct calculation, we can also verify that the principal diffraction directions in this case are parallel and normal to the xz plane. Figure 3 shows the cross section of a Gaussian beam inside this PC structure at different propagation lengths. The beam is assumed to be at normalized frequency of $a/\lambda = 0.45$ with TE polarization (electric field normal to the plane of incidence) and a symmetric shape with a beam waist of 41.2λ upon entrance to the PC structure. Results in Fig. 3(a) are calculated using a direct modal approach based on the plane wave expansion technique as a point of reference, and those in Fig. 3(b) are calculated using our ETF discussed in this paper. The fluctuations on the profile of the beam for the exact method (i.e., the direct modal approach) are caused by the nonuniformity of the refractive index inside the PC structure. It can be observed that the approximate profile calculated by the ETF is an accurate estimate for the envelope of the beam for most practical purposes.

Different broadenings in the two principal directions are also evident from the beam shapes in Fig. 3. Figure

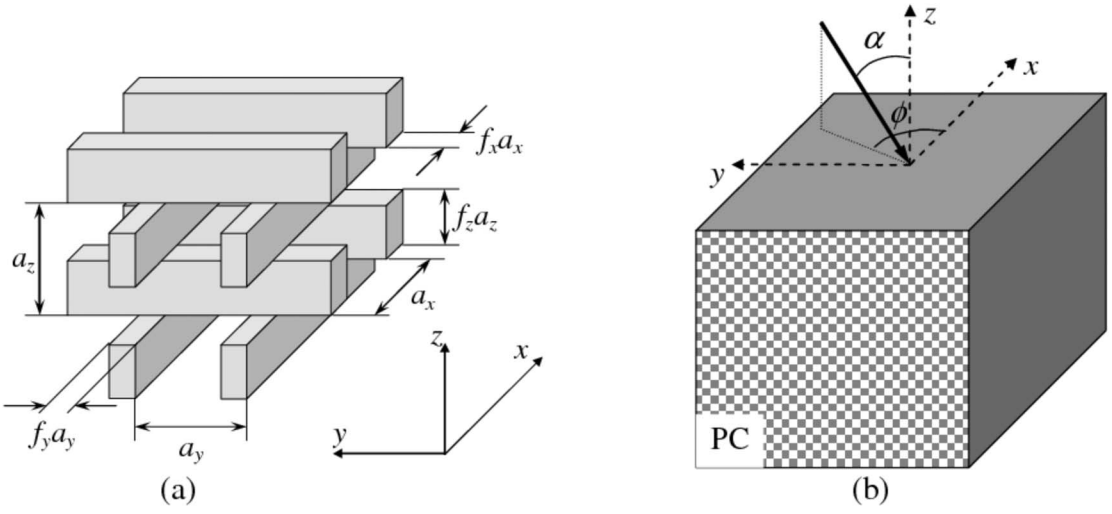

Fig. 2. (a) Schematic of the 3D tetragonal woodpile PC considered throughout this paper is shown. Lattice constants and filling factors in different directions of this lattice are marked in this figure. (b) The general direction of the incident beam is shown, with α being the angle between the incident wavevector and the normal to the interface (z), and ϕ being the angle between the plane of incidence and the xz plane.

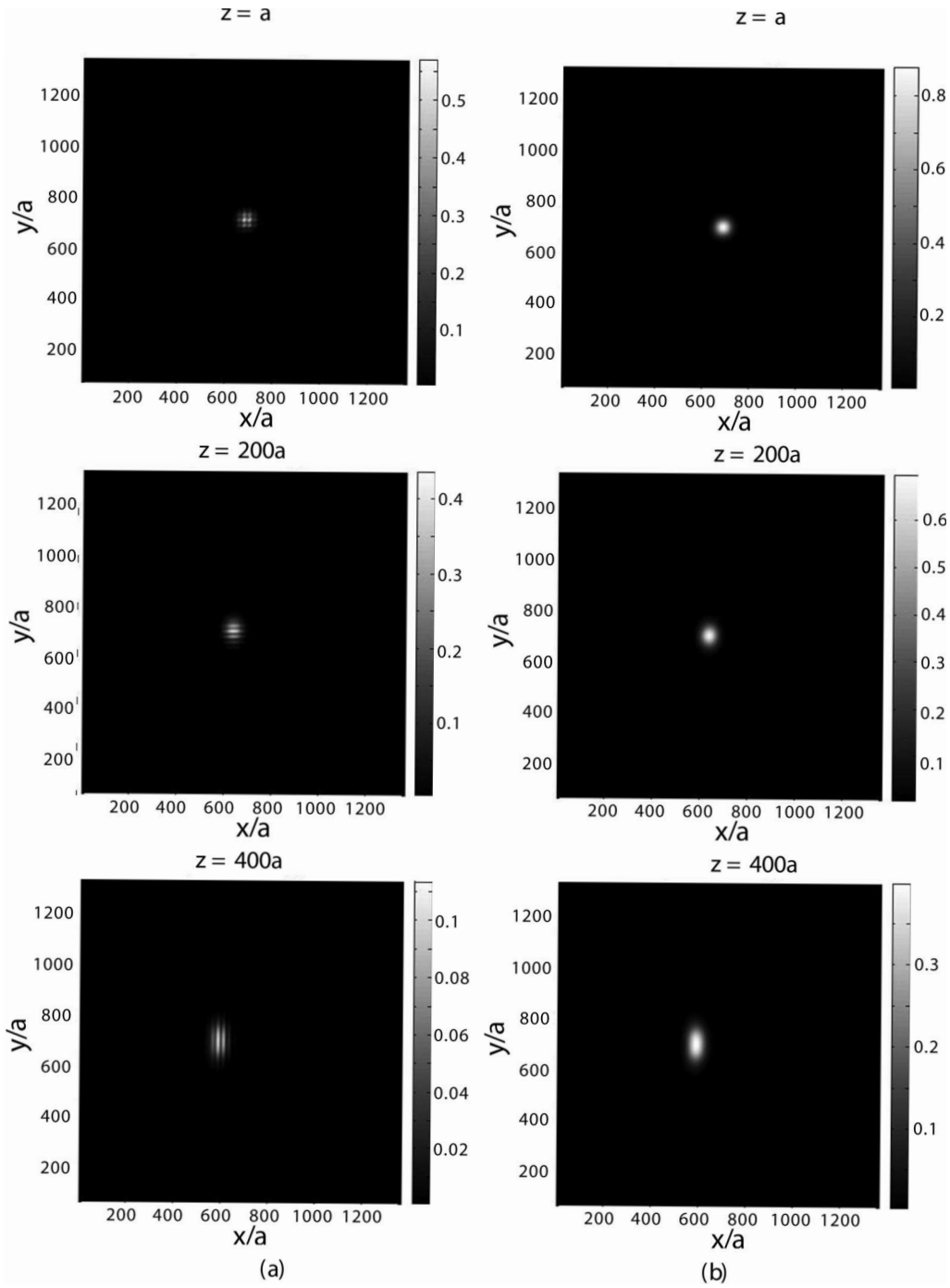

Fig. 3. Calculated cross sections of an optical beam propagating through a tetragonal woodpile PC structure (with $f_x=f_y=0.3$, $f_z=0.5$, and $a=a_x=a_y=a_z/2.4$) are shown at different propagation lengths using (a) the direct mode-matching (brute-force approach) and (b) the ETF approximation. The three snapshots show the calculated E_y field at $z=a$, $200a$, and $400a$, respectively. The beam has a normalized frequency of $a/\lambda=0.45$ and a symmetric beam waist of 41.2λ, and it is incident upon the PC from a homogeneous material with relative permittivity 2.5 at $\alpha=38°$ and $\phi=0°$ as shown in Fig. 2.

3(c) shows the isofrequency surface of the 3D PC used in Figs. 3(a) and 3(b) at the normalized frequency of $a/\lambda=0.45$. The deformation of the bands in the vicinity of the edges of the Brillouin zone is responsible for the anisotropic curvature resulting in the different diffraction of the beam in the x and y directions, as shown in Figs. 3(a) and 3(b). To get a more quantitative result, we have calculated the beam widths in the two principal diffraction directions [i.e., x and y in Fig. 2(b)] at different propagation lengths and the results are shown in Fig. 4. Agreement between the beam widths obtained by the diffractive index model and the ETF technique is clear from Fig. 4. The results in Fig. 4 confirm that the beam width of the propagating beam in the PC structure follows the same simple geometrical optics relation predicted by the diffractive index model.

The possibility of negative diffraction in PC structures is another important property that can affect an optical

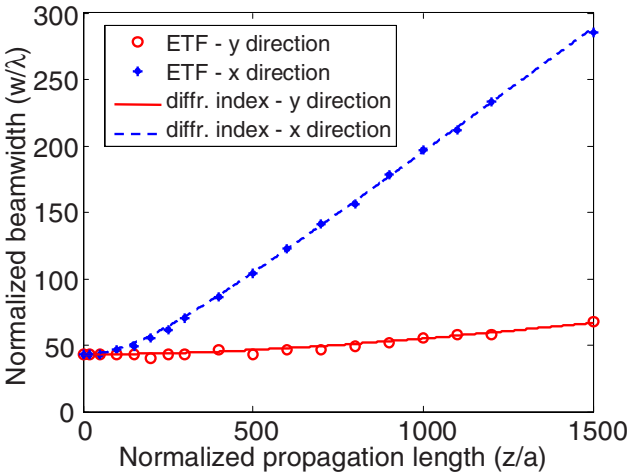

Fig. 4. (Color online) Comparison of the beam widths along the x and y directions for an optical beam propagating inside a 3D PC (same parameters as defined in Fig. 3). The results obtained using the ETF (shown by markers) are in good agreement with the expected beam widths from a diffractive index model (shown by solid curves).

beam propagating inside these structures. The immediate applications of this property are diffraction compensation [18] and beam shaping. To obtain an appropriate 3D PC structure with negative diffraction, we can use our diffractive index model and design the PC structure for the desired diffractive indices along the two principal diffraction directions. More importantly, we can use these indices along with the well-known analytical formulas of geometrical optics to analyze the propagation of the optical beam in such a negative diffraction structure at any arbitrary propagation length. For this analysis, we consider an incident Gaussian beam at the normalized frequency of $a/\lambda=0.57$ with the symmetric beam waist of 20.6λ incident at an angle $\alpha=21.75°$ and $\phi=0°$ from the substrate region on the 3D PC structure in the geometry shown in Fig. 2(b). We choose a woodpile PC structure with $a_x=a_y=a$, $a_z=2.4a$, $f_x=f_y=0.3$, $f_z=0.5$, and $\varepsilon_r=2.5$, similar to the one in Fig. 2. The 3D isofrequency surface for this PC at the operation normalized frequency is shown in Fig. 5(a). The excitation point on the band structure is marked by an arrow in Fig. 5(a), showing that the isofrequency surface at this operation point has different curvatures in the x and y directions. We assume that the beam initially propagates a distance of $L_{\text{pre}}=1960a$ in the substrate with $\varepsilon_r=2.5$ (and thus, broadens to a beam spot of $2w=77\lambda$ in each lateral direction) before entering the PC. The two diffractive indices for this structure at the operation frequency of $a/\lambda=0.57$ are $n_{dx}=-0.16$ and $n_{dy}=0.90$ [calculated from the band structure using Eq. (21)]. The beam profiles normal to the direction of propagation (the z direction) at two different propagation lengths inside the PC structure are shown in Figs. 5(b) and 5(c). Perfect diffraction compensation in the x direction at $L=500a$ is observed from Fig. 5(c), and the transfer-limited spot size is retrieved. Further propagation inside the PC region beyond this point results in the broadening of the beam. It is interesting to note the difference between the diffraction effects in the x and y directions. The beam undergoes normal diffraction in the y direction and continues to broaden upon propagation (since $n_{dy}>0$), while the diffraction effect in the x direction is opposite to that of ordinary bulk materials (since $n_{dx}<0$), and results in focusing of the beam. Figure 5(d) compares the widths of the beam in the x and y directions obtained from direct ETF simulations with those obtained by fitting a Gaussian beam propagation into the calculated data based on a modal analysis. The estimated diffractive indices in the x and y directions from this fitting process are $n_{dx}=-0.14$ and $n_{dy}=0.87$, respectively, which are in good agreement with direct calculations of diffractive indices from the band structure.

It is clear that choosing an appropriate 3D PC structure for diffraction compensation and confirming its effect on the incident beam with direct simulation of propagation (using methods such as FDTD) is very time consuming. This clearly shows the importance of our diffractive index model in the analysis, design, and optimization of 3D PC structures for practical applications.

4. DISCUSSION

The applicability of the diffractive index model is mainly determined by the accuracy of the quadratic approximation of the ETF [Eqs. (10) and (11)]. Any difference between the ETF and our second-order approximation corresponds to diffraction effects during propagation that are ignored in the diffractive index model. Therefore, the error in using the diffractive index model increases by increasing the spatial bandwidth (i.e., range of $\mathbf{k}$) of the incident beam. In most practical applications of 3D PCs (such as wavelength demultiplexing, self-guiding, and diffraction compensation), the incident beam is forced to be collimated (or have a small spatial bandwidth) by the requirements of that application. For such practical cases, the accuracy of our model is very good. Nevertheless, we can improve the accuracy of the model by defining higher-order diffractive indices similar to the two-dimensional case [18] using higher-order approximations to improve the accuracy.

Figure 6 shows beam profile of a Gaussian beam at different propagation lengths in the same structure as the one described in Fig. 5, when the beam waist of the incident light is reduced by a factor of 2 (i.e., the spatial bandwidth is increased by a factor of 2) compared to the incident beam used in the simulations in Fig. 5. The higher-order diffraction effect in this case results in an asymmetrical beam profile and appearance of sidelobes in the output beam profile. Note that again, since the signs of the diffractive index along the x and y directions are different, focusing of the beam along the x direction is observed as opposed to the normal beam broadening along the y direction.

Another possible source of error in our effective diffractive index model is the deviation of the actual situation from the assumption of scalar diffraction used in our model. Noting that the polarization of the incident light is usually fixed, the variation of polarization of the PC modes in the wave-vector excitation range of interest results in reduced coupling efficiency to the PC mode of interest or possibly coupling to other PC modes. However, for almost all 3D PCs of interest for practical applications

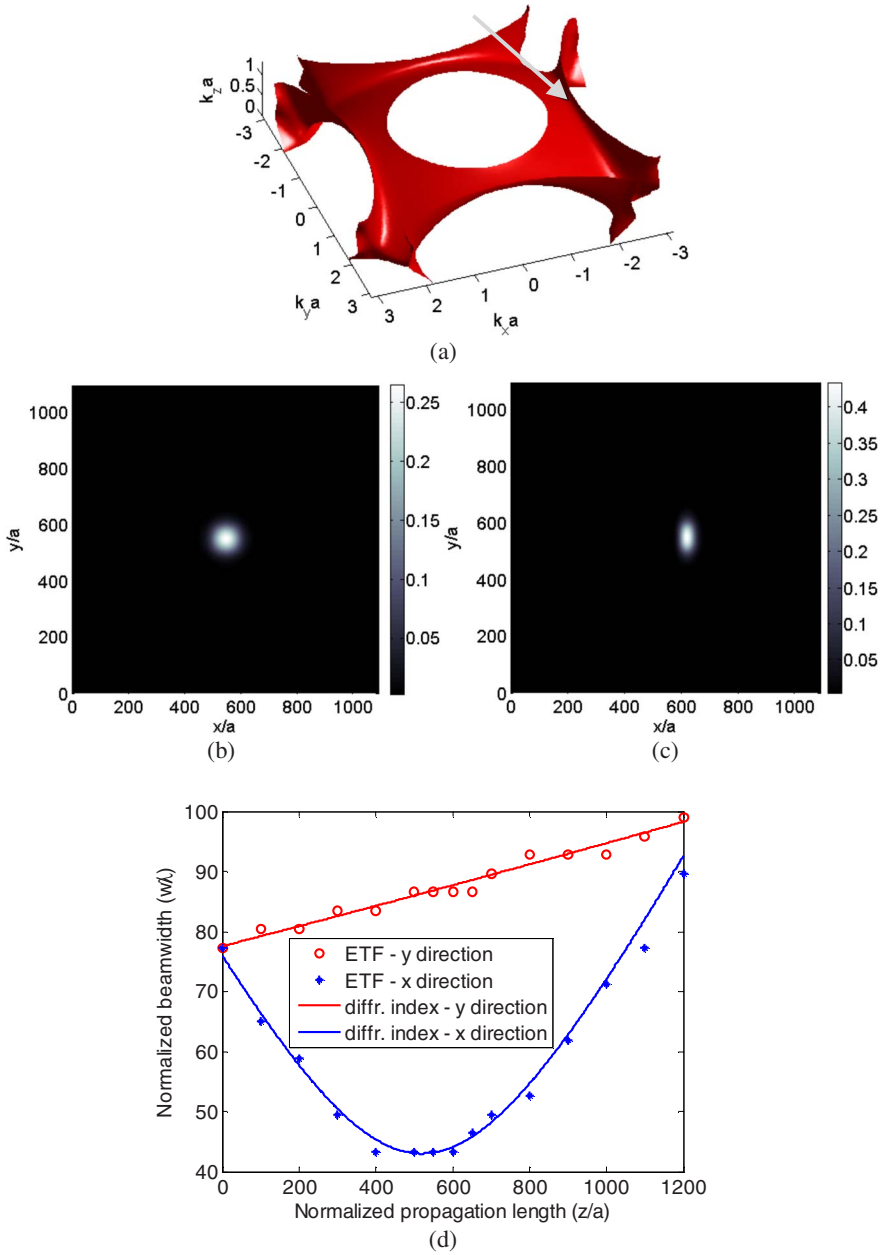

Fig. 5. (Color online) (a) Isofrequency surface of a tetragonal woodpile PC structure (with $f_x=f_y=0.3$, $f_z=0.5$, $\varepsilon_r=2.5$, and $a=a_x=a_y=a_z/2.4$) in the 3D k space at the normalized frequency of $a/\lambda=0.57$ is shown. Only the surface corresponding to the excitation polarization (i.e., E_y) is retained. The excitation is a Gaussian beam incident from the substrate region ($\varepsilon_r=2.5$) at an angle of $\alpha=21.75°$ and $\phi=0°$, with a symmetric beam waist of $2w_0=41.2\lambda$, and is originally broadened to a beam width of 77λ. Cross sections of the beam inside the PC structure is shown at (b) $z=a$ (i.e., upon entrance to the PC region) and (c) $z=500a$. (d) The evolution of the width of the beam during propagation through the PC structure is calculated using the ETF method and our simple diffractive index model, showing good agreement. Using Gaussian beam propagation formulas and by fitting the parameters into the calculated ETF beam widths, the diffractive indices are estimated to be $n_{dx}=-0.14$ and $n_{dy}=0.87$, which are in good agreement with those calculated in our simple model.

in relatively low-index-contrast materials (i.e., woodpile structure, FCC lattice, and diamondlike structure [11] in polymers) PC modes have almost linear polarizations with gradual variations over the band structure [21]. As a result, our model has a good accuracy in analyzing practical structures of interest.

It is important to note that the diffractive index model presented here describes the spatial distribution of the beam during propagation and cannot be used for the analysis of reflection at the interface of 3D PCs with other media. For analyzing the reflection and coupling efficiency, a mode matching scheme can be used at the interface of the PC by including both the propagating and the evanescent modes of the structure [23]. Once the strength of each mode inside the PC structure is found, the propagation of the mode can be analyzed using the diffractive index model.

5. CONCLUSIONS

We demonstrated here an accurate and efficient model based on effective diffractive indices for the analysis of

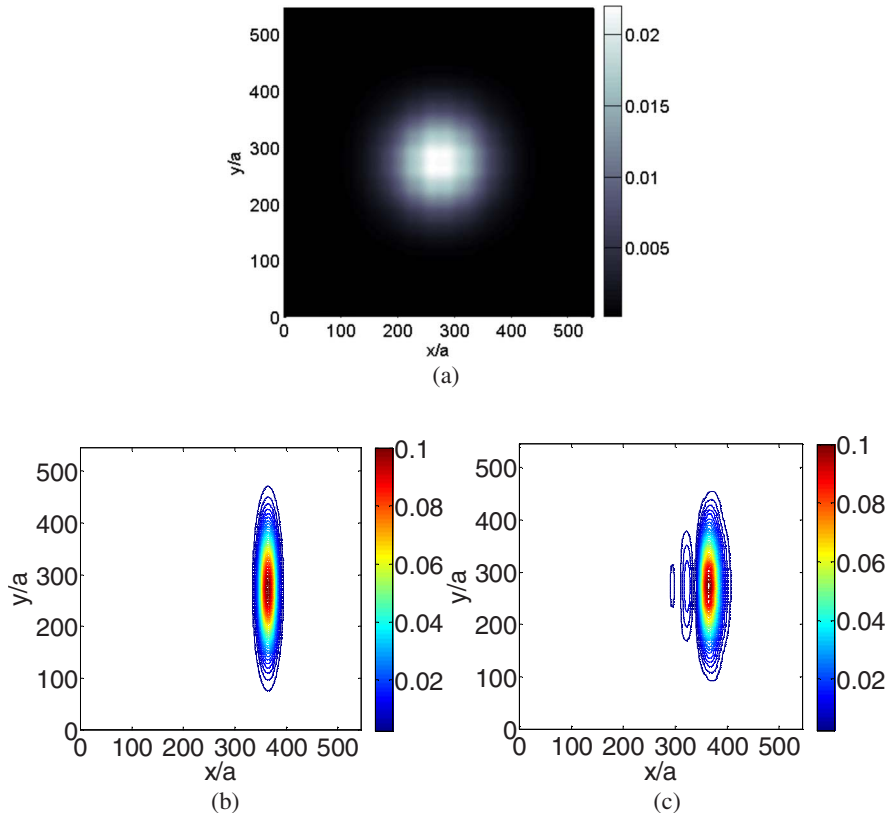

Fig. 6. (Color online) Effect of higher-order diffraction on the profile of a beam inside a tetragonal woodpile PC structure is shown, for the same parameters as those described in Fig. 5, but with an incident beam waist of $2w_0=20.6\lambda$. The cross section of the incident beam at the input inside the PC is shown in (a). The beam profile at $z=650a$ after propagation through the PC with negative diffractive index in the x direction is calculated and its intensity is plotted using (b) the effective index model and (c) the ETF approach. The appearance of sidelobes in the output beam profile in (c) is a result of higher-order diffraction effects that are neglected in the simple effective diffractive index calculations used to find (b).

beam propagation effect inside 3D periodic structures. We showed that two principal diffractive indices (corresponding to two principal diffraction directions) can be defined to describe the propagation of beams in an arbitrary direction inside these structures. The model has good accuracy for the analysis of all 3D PCs of interest for practical applications. Using this method, the beam propagation effects can be studied using simple geometrical optics formulas, which significantly reduces the amount of memory and computation cost needed for the 3D structure compared to other approaches. Thus, the model enables efficient analysis, design, and optimization of 3D PC structures and opens up new possibilities for practical applications of 3D PCs by facilitating their modeling.

ACKNOWLEDGMENT

This work was supported by the Office of Naval Research contract N00014-05-0303. The authors thank M. Spector.

REFERENCES

1. E. Yablonovitch, "Inhibited spontaneous emission in solid-state physics and electronics," Phys. Rev. Lett. **58**, 2059–2062 (1987).
2. S. John, "Strong localization of photons in certain disordered dielectric superlattices," Phys. Rev. Lett. **58**, 2486–2489 (1987).
3. J. Joannopoulos, R. Meade, and J. Winn, *Photonic Crystals: Molding the Flow of Light* (Princeton U. Press, 1995).
4. X. Ao and S. He, "Three-dimensional photonic crystal of negative refraction achieved by interference lithography," Opt. Lett. **29**, 2542–2544 (2004).
5. Z. Lu, S. Shi, C. A. Schuetz, J. A. Murakowski, and D. W. Prather, "Three-dimensional photonic crystal flat lens by full 3D negative refraction," Opt. Express **13**, 5592–5599 (2005).
6. T. Prasad, V. Colvin, and D. Mittleman, "Superprism phenomenon in three-dimensional macroporous polymer photonic crystals," Phys. Rev. B **67**, 165103 (2003).
7. S. Y. Lin, J. G. Fleming, D. L. Hetherington, B. K. Smith, R. Biswas, K. M. Ho, M. M. Sigalas, W. Zubrzycki, S. R. Kurtz, and J. Bur, "A three-dimensional photonic crystal operating at infrared wavelengths," Nature **394**, 251–253 (1998).
8. M. Deubel, G. von Freymann, M. Wegener, S. Pereira, K. Busch, and C. M. Soukoulis, "Direct laser writing of three-dimensional photonic-crystal templates for telecommunications," Nat. Mater. **3**, 444–447 (2004).
9. R. Guo, Z. Li, Z. Jiang, D. Yuan, W. Huang, and A. Xia, "Log-pile photonic crystal fabricated by two-photon photopolymerization," J. Opt. A, Pure Appl. Opt. **7**, 396–399 (2005).
10. M. Deubel, M. Wegener, S. Linden, G. von Freymann, and S. John, "3D-2D-3D photonic crystal heterostructures fabricated by direct laser writing," Opt. Lett. **31**, 805–807 (2006).
11. Y. C. Zhong, S. A. Zhu, H. M. Su, H. Z. Wang, J. M. Chen, Z. H. Zeng, and Y. L. Chen, "Photonic crystal with diamondlike structure fabricated by holographic lithography," Appl. Phys. Lett. **87**, 061103 (2005).
12. J. H. Moon, J. Ford, and S. Yang, "Fabricating three-

dimensional polymeric photonic structures by multi-beam interference lithography," Polym. Adv. Technol. **17**, 83–93 (2006).
13. J. H. Moon, S. Yang, and S.-M. Yang, "Photonic band-gap structures of core-shell simple cubic crystals from holographic lithography," Appl. Phys. Lett. **88**, 121101 (2006).
14. J. Chen, W. Jiang, X. Chen, L. Wang, S. Zhang, and R. T. Chen, "Holographic three-dimensional polymeric photonic crystals operating in the 1550 nm window," Appl. Phys. Lett. **90**, 093102 (2007).
15. R. Zengerle and P. C. Hoang, "Photonic crystal structures for potential dispersion management in optical telecommunication systems," Proc. SPIE **5595**, 78–91 (2004).
16. B. Momeni and A. Adibi, "An approximate effective index model for efficient analysis and control of beam propagation effects in photonic crystals," J. Lightwave Technol. **23**, 1522–1532 (2005).
17. B. Momeni and A. Adibi, "Optimization of photonic crystal demultiplexers based on superprism effect," Appl. Phys. B **77**, 556–560 (2003).
18. B. Momeni and A. Adibi, "Preconditioned superprism-based photonic crystal demultiplexers: analysis and design," Appl. Opt. **45**, 8466–8476 (2006).
19. J. Shin and S. Fan, "Conditions for self-collimation in three-dimensional photonic crystals," Opt. Lett. **30**, 2397–2399 (2005).
20. J. Mizuguchi, Y. Tanaka, S. Tamura, and M. Notomi, "Focusing of light in a three-dimensional cubic photonic crystal," Phys. Rev. B **67**, 075109 (2003).
21. M. Badieirostami, B. Momeni, and A. Adibi, are preparing a paper to be called "Polarization state for modes of low-contrast three-dimensional photonic crystal structures."
22. J. J. Stoker, *Differential Geometry* (Wiley, 1969), Chap. 4.
23. B. Momeni, M. Badieirostami, and A. Adibi, "Accurate and efficient techniques for the analysis of reflection at the interfaces of three-dimensional photonic crystals," J. Opt. Soc. Am. B **24**, 2957–2963 (2007).